



Study of Coulomb Stress Change (CSC) Earthquake in the Segment Area of West Seram – Ambon Island

Matheus Souisa^{1,2,3,4*}, Sisca Madonna Sapulete^{1,2,3,4}, Stenly Samalelaway¹

¹Department of Physics, Faculty of Mathematics and Natural Sciences, University of Pattimura, Ambon, Indonesia.


²Landslides Laboratory, Faculty of Mathematics and Science, University of Pattimura, Ambon, Indonesia.

³Disaster Mitigation Laboratory, Faculty of Mathematics and Science, University of Pattimura, Ambon, Indonesia.

⁴Geosciences Center, Faculty of Mathematics and Science, University of Pattimura, Ambon, Indonesia

Received: August 16, 2022
Revised: October 18, 2022
Accepted: October 27, 2022
Published: October 31, 2022

Corresponding Author:
Matheus Souisa
thos.phys@gmail.com

© 2022 The Authors. This open access article is distributed under a (CC-BY License) 

DOI: [10.29303/jppipa.v8i4.2025](https://doi.org/10.29303/jppipa.v8i4.2025)

Abstract: The earthquake that occurred on September 26, 2019, at 08:46:45 WIT with a magnitude of 6.5 on the Richter Scale in parts of West Seram Island facing Ambon Island suddenly shook the area around the epicenter. The purpose of this study was to determine the CSC of the SBB – Ambon Island earthquake in 2019 and the effect of the main earthquake stress release on aftershocks. The results showed that the main SBB earthquake - Ambon Island on September 26, 2019, with a depth of 12.7 km, caused aftershocks. In the decreasing lobe, the Coulomb stress value changes from around -0.1 bar to 1.0 bar which is located on the right and left of the fault plane at a depth of up to 30 km. The distribution of Coulomb stress changes in the SBB earthquake - Ambon Island is depicted by the dominant positive lobe occurring at the side end of the fault plane, while the dominant negative lobe occurs in the area perpendicular to the fault plane due to the influence of the dominant earthquake source mechanism in the form of strike-slip.

Keywords: Coulomb stress changes; earthquakes; Seram-Ambon Island segment

Introduction

One of the areas in Maluku Province that is prone to earthquakes is Seram Island. Seram Island is located between the confluence of the continental crust of Australia, the crust of the Eurasian Continent, and the crust of the Pacific Ocean. There are two fault systems that border Seram Island, namely the fault system in the north of Sorong and the Tarera-Aiduna fault in the south. Seram Island is formed from rising faults with sharp angles to horizontal faults and has a complex tectonic setting, which is generally in the form of rising faults and anticline axis trending northwest-southeast (Kumparan, 2019).

According to the Meteorology, Climatology and Geophysics Agency (BMKG), the earthquake that occurred on Seram-Ambon Island on September 26, 2019, was a shallow earthquake with coordinates 128.39 °E, 3.53 °S and a depth of 10 km. This is caused by the

movement of local faults, namely horizontal faults. The main earthquake that occurred had a magnitude of 6.5 on the Richter scale, and the aftershocks had the strongest magnitude of 5.6 on the Richter Scale (Sipayung, 2020).

To understand whether an earthquake with a magnitude of 6.5 on the Richter scale in the West Seram (SBB)-Ambon Island segment changes the surrounding area to failure in the West Seram Bay fault system, by discussing the general problem of how one earthquake can trigger another. Earthquakes themselves occur due to the release of rock stress. So that when the elastic limit of the rock is exceeded, there is a release of energy because the rock is no longer able to withstand stress (Setiadi et al., 2017).

To understand whether earthquakes with magnitude The tendency of rocks to collapse in a brittle manner is considered a function of shear stress and stress, which are generally formulated as Coulomb

How to Cite:

Souisa, M., Sapulete, S.M., & Samalelaway, S. (2022). Study of Coulomb Stress Change (CSC) Earthquake in the Segment Area of West Seram – Ambon Island. *Jurnal Penelitian Pendidikan IPA*, 8(4), 2012-2018. <https://doi.org/10.29303/jppipa.v8i4.2025>

failure criteria. It can be explored how changes in Coulomb conditions associated with one or more earthquakes can trigger subsequent events. First consider the appropriate Coulomb criteria for the production of aftershocks, where the faults most likely to slip are failure-oriented as a result of the prevailing regional stress field and stress changes caused by the main shock. Thus, the distribution of earthquake occurrence patterns can be studied using the Coulomb Stress Change (CSC) method approach.

Method

Research area

Earthquake data collection was carried out at the Meteorology, Climatology and Geophysics Agency office, Ambon area, namely before the earthquake occurred until the earthquake ended. Geographically, the research location is located at coordinates 3°19'56.90" South Latitude - 3°41'20.53" South Latitude to 128° 9'1.24" East Longitude - 128°30'38.68" East Longitude.

The model of Coulomb stress change

The shear stress t in the fracture must exceed the critical value T as a linear function of the normal stress. This is based on the Mohr-Coulomb collapse (Navas-Portella et al., 2020, Souisa and Sapulete, 2021).

In predicting the distribution of seismicity, a physical approach can be used by modeling the change in Coulomb stress (Cocco and Rice, 2002; Toda et al., 2005). The calculation model using the Coulomb voltage change (Souisa and Sapulete, 2021) is,

$$CSC = \Delta\tau + \mu' \Delta\sigma_n \tag{1}$$

where $\Delta\sigma_n$ is the normal stress (positive unclamping) and $\mu' = \mu(1-B)$ is the apparent coefficient of friction of the fault rupture plane.

The failure plane (Figure 1) is subjected to a primary stress component (σ_n), which can produce a shear stress in the failure plane. The orientation of the primary stress to the angle (β) in the failure plane will increase (σ_1) and decrease (σ_3) the stress in the failure plane (Souisa and Sapulete, 2021). Calculation of CSC on rock faults due to earthquakes depends on the geometry and distribution of the slip, the magnitude of the assumptions, the orientation of regional stresses, and the assumed value of the friction coefficient. In some earthquake events, the uncertainty of the CSC is always dominated by the uncertainty of the slip distribution.

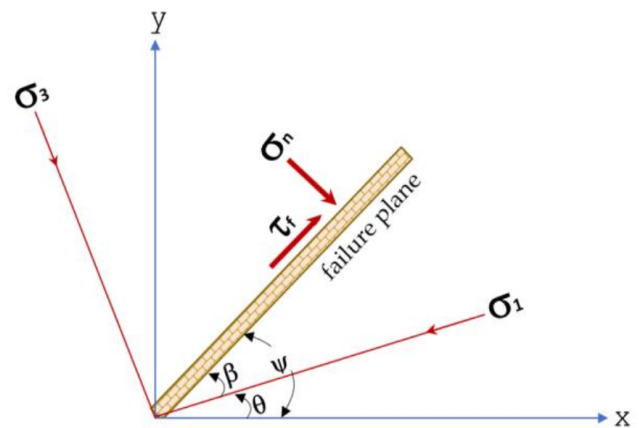


Figure 1. Coulomb stress calculation on failure plane by applying a coordinate system (King, 2014, Souisa and Sapulete, 2021).

Result and Discussion

Data processing

CSC modeling using fault parameter input shows the inversion of aftershocks promoted by positive CSC at shallow depths (0 - 20,0) km. The map shows the distribution of aftershocks $M > 5.0$, which is considered to have a greater epicenter uncertainty. This aftershock needs to be relocated again to improve the depth of the hypocenter. On the other hand, aftershocks in the Northwest-Southeast part of the fault (in the Seram Strait) are more suitable to be promoted by positive CSC at a normal depth of 12.7 km and carried out at a depth of 20.0 km.

Main earthquake and aftershocks > 5.0 SR in 2019

The main earthquake and aftershocks > 5.0 SR that occurred in 2019 were obtained from the results of the Global CMT and USGS calculations which were then verified with BMKG data (Table 1). Parameters from this earthquake are used to calculate CSC and display a cross-section of stress changes that occur due to earthquakes or display the dispersion pattern of rock CSC vertically based on depth. The earthquake source mechanism issued by the three institutions shows compatibility with one another, namely the earthquake caused by a strike-slip type fault at shallow depths in the crust (crustal earthquake). Calculation of the CSC and the effect of stress release using two types of fault parameters. The fault parameter in the first nodal section is the result of a horizontal fault in a north-south direction with an almost vertical dip with right lateral movement. And in the second nodal plane is the result of left-lateral movement in an East-West direction. This calculation uses the coefficient of friction (friction) of 0.4. The coefficient of effective friction is between 0.0 and 0.8 for most faults (Lin et al., 2019).

Table 1. Parameters of the main earthquake and aftershocks in 2019 > 5.0 SR

Time	Epicenter (°)	Depth (km)	Mag (Mw)	Strike (°)	Dip (°)	Rake (°)
26/09/2019	128.39 dan -3.54	12.7	6.5	345 253	78 84	-174 -12
27/09/2019	128.45 dan -3.54	12.0	5.5	229 15	40 56	-62 -111
11/10/2019	128.28 dan -3.54	14.0	5.2	263 358	68 78	-13 -158
13/11/2019	128.33 dan -3.54	13.4	5.2	270 4	73 77	-13 -162

Model of CSC of the main earthquake on September 26, 2019

a. For normal conditions (12.7 km)

CSC model as shown in Figure 2, was carried out on two different fault parameters, namely strike angle, dip and rake with normal depth (12.7 km).

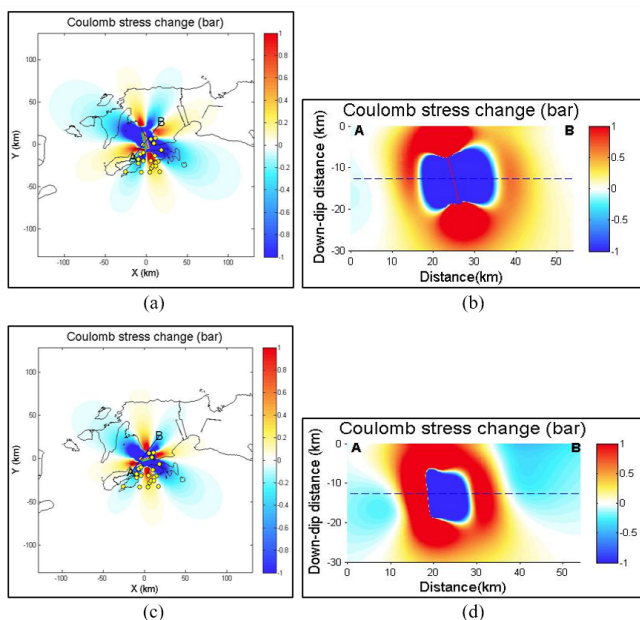


Figure 2. CSC and cross-section of the September 26, 2019 earthquake. (a). CSC with fault parameters (strike 345°, dip 78°, rake -174°) at a depth of 12.7 km, (b). Cross-section with fault parameters (strike 345°, dip 78°, rake -174°) at a depth of 12.7 km, (c). CSC with fault parameters (strike 253°, dip 84°, rake -12°) at a depth of 12.7 km, (d). Cross-section with fault parameters (253° strike, 84 dip, -12° rake) at a depth of 12.7 km.

Figure 2(a) shows the shape of the fault leading from North-Northwest to South-Southeast, and the CSC that occurs is quite large with a positive value (4 lobes in red) in the direction of North-Northwest, East-Northeast, South -Southeast, and West, with stress values ranging from 0.1 bar to 1.0 bar. Meanwhile, the CSC that occurs is quite large with a negative value (4 lobes in blue) in the Northwest, North-Northeast, Southeast - Northwest and in the Northeast - Southwest, with a decreasing stress change value in the range of -0.1 bar to -1.0 bar. As for Figure 2c, the fault points from East - Northeast to West - Southwest, and the CSC that occurs is quite large with positive values (4 lobes in red)

in the North, South, East - Northeast, and West directions, with stress values ranging from 0.1 bar to 1.0 bar. Meanwhile, there was a decrease in negative CSC (4 lobes in blue) in the Northwest, Southeast, Northeast and Southwest directions, with stress values ranging from -0.1 bar to -1.0 bar.

Figures 2(a) and 2(c), show that the vertical coulomb stress distribution pattern which shows the hypocenter of an earthquake with a depth of 12.7 km has a large enough increase in coulomb stress of about 1 bar (0.1 MPa) which can be This means that aftershocks are likely to occur with a fairly high frequency and large magnitude. In areas with decreased stress (blue lobes) tend to provide balance in areas with increased stress (red lobes) (Mala and Mohamad, 2020).

For modeling the distribution of CSC in rock vertically with depth, a cross-section at a depth of 30 km and a length of 50 km was used (Figures 2b and 2d). When viewed from the cross-section (Figure 2(b)), the first aftershock occurred at a distance of 45.0 km towards the South with a depth of 12.7 km below the earth's surface. According to the cross-section, this earthquake is in an area of increased Coulomb stress (red lobe) it is possible that the earthquake was triggered (triggered) by the main earthquake on September 26 which caused aftershocks (faults) and made it possible for another aftershock to occur. in the future in areas with positive stress at a depth of 30.0 km with a distribution of CSC ranging from (0.1 - 1.0) bar or equivalent to (0.01 - 0.1) MPa. The same thing is also seen in the cross-section (Figure 2(d)), and the difference is that the first aftershocks occurred at a distance of 40.2 km towards the South with a depth of 30.0 km below the earth's surface.

b. Depth variation (10.0 km and 20.0 km)

The modeling of CSC as shown in Figure 3, was carried out in one nodal plane with fault parameters such as strike 253°, dip 84°, rake -12° with a depth of 10.0 km, and fault parameters in the form of strike 345°, dip 78°, rake -174° with a depth of 20.0 km. Figure 3(a) shows the shape of the fault leading from North - Northwest to South - Southeast, and the CSC that occurs is quite large with positive values (4 lobes in red) in the East, West, North - Northwest, and South - Southeast, with the stress value increasing from 0.1 bar to 1.0 bar. Meanwhile, the CSC that occurs is quite large with

negative values (4 lobes in blue) in the Northwest, Southeast, Northeast, and Southwest directions, with the stress value decreasing from -0.1 bar to -1.0 bar.

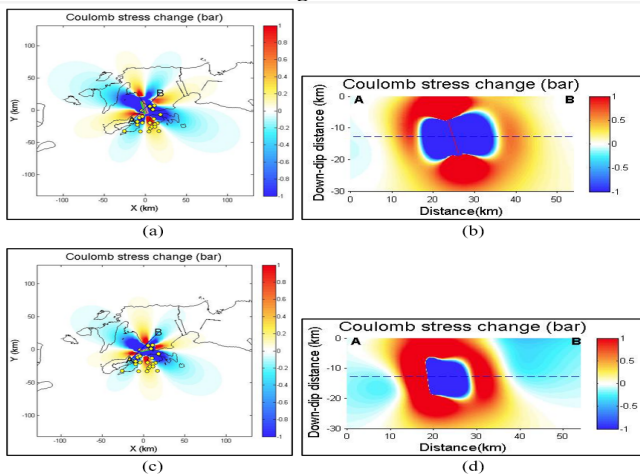


Figure 3. (a). CSC with fault parameters (strike 345°, dip 78°, rake -174°) with a depth variation of 10.0 km, (b). Cross-section with fault parameters (strike 345°, dip 78°, rake -174°) with a depth variation of 10.0 km, (c). CSC with fault parameters (strike 345°, dip 78°, rake -174°) with a depth variation of 20.0 km, (d). Cross-section with fault parameters (strike 345°, dip 78°, rake -174°) with a depth variation of 20.0 km.

As for Figure 3c, the fault points from North - Northwest to South - Southeast, and the CSC that occurs is quite large with positive values (4 lobes in red) in the East, West, North - Northwest, and South - Southeast directions with an increase in the value of the change in stress ranges from 0.1 bar to 1.0 bar. CSC that occurs is quite large with negative values (4 lobes in blue) being in the West-Northwest, East-Southeast, North-Northeast, and in the South-Southwest direction, with a decrease in the value of the stress change from -0.1 bar to -1.0 bar.

For modeling the distribution of CSC in rock vertically with depth, a cross-section at a depth of 30.0 km and a length of 50.0 km (Figures 3b and 3d). If viewed from the cross-section (Figure 3(b)), the first aftershock occurred at a distance of > 50.0 km tending to the south with a depth of 30.0 km. The same thing is also seen in the cross-section (Figure 3(d)), and the difference is that the first aftershocks occurred at a distance of < 35.5 km tending to the north with a depth of 30.0 km. By cross-section, this earthquake is located in the relaxation area which allows the probability of failure to be greater, so the occurrence of earthquakes that may occur in the relaxation area tends to increase.

The model of CSC for the September 27, 2019, aftershock

a. For normal conditions (12.0 km)

The earthquake that occurred on September 27, 2019 with Mw 5.5 on the Richter Scale was influenced by a strike-slip fault as shown in (Figure 4), the change in rock stress resulted in a change pattern displayed in the

positive lobe area indicating an increase in Coulomb stress and in the lobe area. negative indicates a decrease in Coulomb stress.

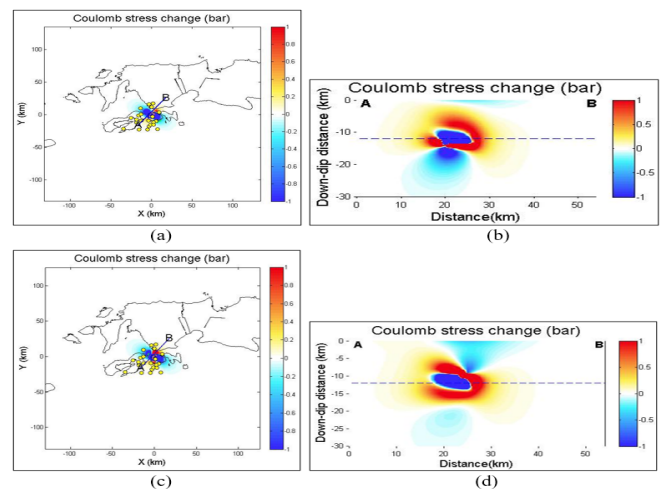


Figure 4. CSC and cross-section of the September 27, 2019 earthquake. (a). CSC with fault parameters (strike 229°, dip 40°, rake -62°), at a depth of 12.0 km, (b). Cross-section with fault parameters (strike 229°, dip 40°, rake -62°), at a depth of 12.0 km, (c). CSC with fault parameters (strike 15°, dip 56°, rake -111°) at a depth of 12.0 km, (d). Cross-section with fault parameters (strike 15°, dip 56°, rake -111°) at a depth of 12.0 km.

The CSC model as shown in Figure 4, was carried out on two different fault parameters with a depth of 12.0 km. Figure 4. (a) shows the shape of the fault leading from Southwest to Northeast and the change in Coulomb stress that occurs is quite large with positive values (3 lobes in red) in the Northeast, West and Southwest directions, with stress values increasing from 0.1 bar to 1.0 bar. Meanwhile, the CSC that occurs is quite large with a negative value (2 lobes in blue) in the Northwest and Southeast directions with the stress value decreasing from -0.1 bar to -1.0 bar. As for Figure 4c, the fault is from Northeast to Southwest, and the CSC that occurs is quite large with a positive value (2 lobes in red) in the Northeast and South-Southwest directions, with the stress value increasing from 0.1 bar to 1.0 bar. Meanwhile, the CSC that occurs is quite large with a negative value (2 lobes in blue) in the Northwest and Southeast directions with the stress value decreasing from -0.1 bar to -1.0 bar.

Based on the cross-section (Figure 4. (b)), the first aftershocks occurred at a distance of < 30.0 km in the direction of South and North with a depth of 30.0 km below the earth's surface. The same thing is also seen in the cross-section (Figure 4. (d)), and the difference is that the first aftershock occurred at a distance of < 28.0 km in the direction of South and East with a depth of 30.0 km below the earth's surface. Following the cross-section, this earthquake is in an area of increased coulomb stress (red lobe) it is possible that the earthquake was triggered by the main earthquake which caused aftershocks and allowed another aftershock to occur again in the future.

b. Depth variation (10.0 km and 20.0 km)

The modeling of CSC as shown in Figure 5, was carried out on fault parameters (strike 229°, dip 40°, rake -62°) with depth variations of 10.0 km and 20.0 km. Figure 5. (a) shows the shape of the fault leading from Southwest to Northeast, and the CSC that occurs is quite large with positive values in the North and South directions, with stress values increasing from 0.1 bar to 1.0 bar. Meanwhile, the change in Coulomb stress that occurs is quite large with negative values in the Northwest and Southeast directions with the stress value decreasing from -0.1 bar to -1.0 bar. As for Figure 5.c, the fault is from Southwest to Northeast and the CSC that occurs is quite large with positive values in the Northeast and South-Southwest directions, with stress values increasing from 0.1 bar to 1.0 bar. While the CSC that occurs is quite large with negative values in the Southwest and Southeast directions with the stress value decreasing from -0.1 bar to -1.0 bar.

If viewed from the cross-section (Figure 5(b)), the first aftershock occurred at a distance of about 28.0 km in a south direction with a depth of 30.0 km below the earth's surface, although the cross-section shows that this earthquake was in an area relaxation which allows the probability of failure to increase, so that the number of earthquakes that may occur in the relaxation area tends to increase. The same thing is also seen in the cross-section (Figure 5(d)), and the difference is that the first aftershock occurred at a distance of about 38.5 km towards the North with a depth of 20.0 km below the earth's surface. According to the cross-section, this earthquake is in an area of increased coulomb stress (red color) which means that it is possible that the earthquake was triggered by the main earthquake that caused aftershocks and it is still possible for another aftershock to occur.

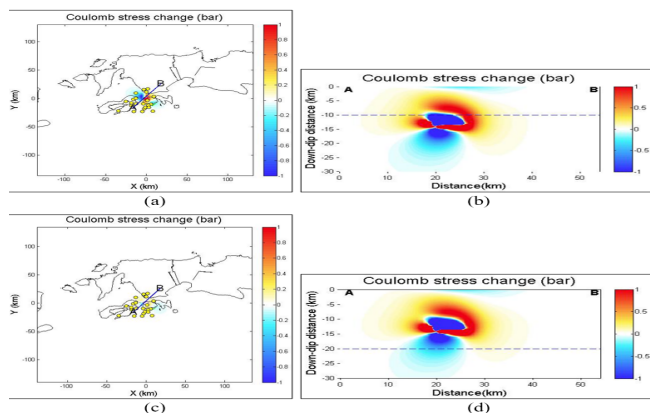


Figure 5. CSC and cross-section of the September 27, 2019 earthquake. (a). CCS with fault parameters (strike 229°, dip 40°, rake -62°) with a depth of 10 km, (b). Cross-section with fault parameters (strike 229°, dip 40°, rake -62°) with a depth of 10 km, (c). CSC with fault parameters (strike 229°, dip 40°, rake -62°) with a depth of 20 km, (d). Cross-section with fault

parameters (strike 229°, dip 40°, rake -62°) with a depth of 20 km.

Implications of the 2019 Ambon tectonic earthquake on rock CSC and aftershocks

The 2019 Ambon earthquake which was intraplate was preceded by a series of initial earthquakes (foreshocks). Usually, the initial earthquake appears in January in the northern part near the initial break of the main earthquake, then stops in March-May 2019. Foreshocks reappear in this northern zone in June-September 2019, and their activity increases until the initiation of the main earthquake. This is clearly seen in the spatial and temporal distribution and cumulative number (Figure 6).

The productivity of the aftershocks in the case of the 2019 Ambon earthquake is quite high (Sianipar et al., 2020). This may be caused by the main earthquake which has a low-stress drop value (< 0.1 MPa). According to Wetzler et al. (2016), earthquakes with low-stress drops tend to produce more aftershocks. The model shows that the 2019 Ambon earthquake occurred on a fault with a right lateral strike-slip type in a south-north direction. This fault is estimated to be between the islands of Ambon and Haruku extending to the north around the southwest of Kairatu, Seram Island. As mentioned above, the existence of strike-slip and thrust structures is a natural thing around Seram Island as a form of accommodation for complex deformations (Watkinson and Hall, 2017).

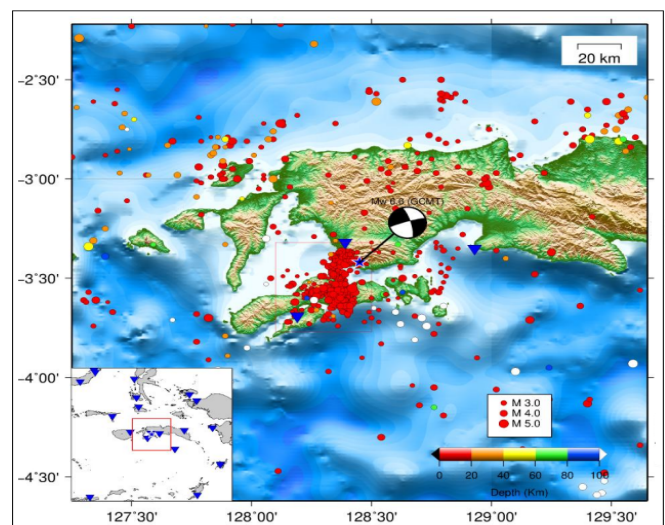


Figure 6. Seismicity around the western part of Seram Island, Maluku, Indonesia from 1 January - 18 October 2019 (source: www.inatews.bmkg.go.id). Beachball shows the mechanism for September 26, 2019, Ambon earthquake (GCMT).

The earthquake had a significant impact on the surrounding area, namely the stress load on the eastern segment of the Seram Strait fault zone had exceeded the threshold to trigger aftershocks (Toda et al. 2005; Parsons et al. 2006; Parsons et al. 2008). In addition, CSC

calculations show that the Ambon earthquake only occurred in the positive stress change area of the 2019 Ambon main earthquake. Of course, the calculation of the stress change depends on the slip model, receiver error, and other parameters, such as depth and effective friction coefficient, which causes some differences. In displaying results (Wan et al., 2000; Miao and Zhu, 2012). Nonetheless, it was observed that the increased stress in and around the epicentral area of the Ambon earthquake (27 September 2019) due to the 26 September 2019 Ambon earthquake was large enough to trigger a series of aftershocks. The aftershock on September 27, 2019, experienced a fault shift of 7.0 km from the main earthquake.

Conclusion

Based on the results of the research and discussion that have been stated, it can be concluded that: (1) The modeling results obtained that the main SBB earthquake - Ambon Island on September 26, 2019 with a depth of 12.7 km, caused aftershocks. Modeling the main earthquake just above the fault plane at a depth of 12.7 km and aftershocks of about 10.0 km and 12.0 km, the Coulomb stress values were identified as homogeneous ranging from (0.1 to 1.0) bar. Furthermore, just below the fault plane at a depth of about 10 km and 20.0 km, an area of significant increase in Coulomb stress was identified at (0.1 - 0.5) bar; (2) The distribution of CSC in the SBB - Ambon Island earthquake, in Figures 2 - 4, shows the dominant positive stress ranging from (0.1 - 1.0) bar and the dominant negative stress ranging from -0.1 bar to 1.0 bar. Most of the aftershock's distribution is concentrated in the area of increased Coulomb stress with a range of (0.1 - 0.8) bar and is located to the southeast of the fault plane.

Acknowledgements

Thanks to BMKG Ambon for preparing earthquake data, and the Geoscience Center FMIPA, Pattimura Universities that have prepared facilities for data analysis, and all parties who have supported completion of this research.

References

- Cocco, M., & Rice, J. R. (2002). Pore pressure and poroelasticity effects in Coulomb stress analysis of earthquake interactions. *Journal of Geophysical Research: Solid Earth*, 107(B2), ESE 2-1-ESE 2-17. <https://doi.org/https://doi.org/10.1029/2000JB000138>.
- King, G.C.P. (2014). Static Stress Changes and the Triggering of Earthquakes by King, G.C.P., Stein, R.S. & Lin, J. (1994). Bulletin of the Seismological Society of America, 84(3), 935-953. Retrieved from <https://www.researchgate.net/publication/23700715>.
- Kumbaran. (2019). *Mengenal Kondisi Geologi Pulau Seram: Ambon, Maluku*, diakses pada tanggal 15 September 2020. Retrieved from: <https://kumbaran.com/...1rwktbBY8R0/full>.
- Lin, X., Chu, R. and Zeng, X. (2019). Rupture processes and Coulomb stress changes of the 2017 Mw 6.5 Jiuzhaigou and 2013 Mw 6.6 Lushan earthquakes. *Earth, Planets and Space, Springer Open*, 71(1), 81. <https://doi.org/10.1186/s40623-019-1061-3>.
- Mala, H. U., & Mohamad, J. N. (2020). Arah Penyebaran Stres Coulomb Pada Batuan Akibat Gempabumi Kairatu 26 September 2020, *Wahana Fisika*, 5(1), 62-70. Doi: <https://doi.org/10.17509/wafi.v5i1.24500>.
- Miao, M., & Zhu, S. (2012). A study of the Impact of Static Coulomb Stress Change of Megathrust Earthquakes Along Subduction Zona on the Following Aftershocks, *Chines Journal of Geophysics*, 55(5), 539-551. <https://doi.org/https://doi.org/10.1002/cjg2.1748>.
- Navas-Portella, V., Jiménez, A., & Corral, Á. (2020). Significant Effect of Coulomb Stress on Gutenberg-Richter Law after the Landers Earthquake. *Scientific Reports*, 10(1), 2901. <https://doi.org/10.1038/s41598-020-59416-2>.
- Parsons, T., Yeats, R.S., Yagi, Y., & Hussain, A. (2006). Static stress change from the 8 October, 2005 M = 7.6 Kashmir earthquake, *Eophysical Research Letters*, VOL. 33(6), 1-4. <https://doi.org/https://doi.org/10.1029/2005GL025429>
- Parsons, T., Ji, C., & Kirby, E. (2008). Stress changes from the 2008 Wenchuan earthquake and increased hazard in the Sichuan basin, *Nature*, 454(7203), 509-510. <https://doi.org/https://doi.org/10.1029/2005GL025429>.
- Setiadi, T.A.P., Perdana, Y.H., & Rohadi, S. (2017). Analisis Coulomb Stress Gempa Bumi Deli Serdang 16 Januari 2017, *Prosiding Seminar Nasional Fisika*, 6, 57-64. doi: <https://doi.org/10.21009/03.SNF2017.02.EPA.09>.
- Sianipar, D., Halauwet, Y., Daryono. & Karnawati, D. (2019). Studi Sumber Gempa Ambon 26 September 2019 Mw 6,5. BMKG. doi: <https://doi.org/10.31227/osf.io/6e9nm>.
- Sipayung, F.S.P. (2020): *Relokasi Hiposenter Gempa Ambon 26 September 2019 Menggunakan Metode Double-Difference*. <https://library.universitaspertamina.ac.id/xmlui/handle/123456789/2052>
- Souisa, M. and Sapulete, S.M. (2021): Analysis of the impact of Coulomb stress changes of Tehoru earthquake, *Jurnal Penelitian Pendidikan IPA (JPPIPA)*, 7(4). <https://doi.org/10.29303/jppipa.v7i4.975>.

- Toda, S., Stein, R., Richards-Dinger, K., & Bozkurt, S. (2005). Forecasting the evolution of seismicity in Southern California: Animations built on earthquake stress transfer. *Journal of Geophysical Research B: Solid Earth*, 110(5), 1-17. doi: <https://doi.org/10.1029/2004JB003415>
- Wan, Y. G., Wu, Z. L. and Zhou, G.W. (2000): Stress triggering" between different rupture events in several earthquakes. *Acta Seismologica Sinica* (in Chinese), 22(6), 568-576. doi: <https://doi.org/10.1007/s11589-000-0062-3>.
- Watkinson, I.M., & Hall, R. (2017). Fault systems of the eastern Indonesian triple junction: evaluation of Quaternary activity and implications for seismic hazards. *Geological Society, London, Special Publications*, 441(1), 71-120. <https://www.lyellcollection.org/doi/10.1144/sp441.8>
- Wetzler, N., Brodsky, E.E., & Lay, T. (2016). Regional and stress drop effects on aftershock productivity of large megathrust earthquakes, *Geophysical Research Letters*, 43(23), 1-9. <https://agupubs.onlinelibrary.wiley.com/doi/full/10.1002/2016GL071104>